Photodiagnosis and Photodynamic Therapy 25 (2019) 463–471

Contents lists available at ScienceDirect

Photodiagnosis and Photodynamic Therapy

journal homepage: www.elsevier.com/locate/pdpdt

# Bright spot analysis for photodynamic diagnosis of brain tumors using confocal microscopy

Takeshi Yoneyama[a,*], Tetsuyo Watanabe[a], Sho Tamai[b], Katsuyoshi Miyashita[b], Mitsutoshi Nakada[b]

[a] School of Mechanical Engineering, Kanazawa University, Kakuma-machi, Kanazawa 920-1192, Japan
[b] Department of Neurosurgery Graduate School of Medical Science, Kanazawa University, Takara-machi, Kanazawa 920-8641, Japan

ARTICLE INFO

*Keywords:*
Neurosurgery
Photodynamic diagnosis
Brain tumor
Fluorescence intensity
Confocal microscope

ABSTRACT

*Background:* In a previous study of photodynamic tumor diagnosis using 5-aminolevulinic acid (5-ALA), the authors proposed using fluorescence intensity and bright spot analyses under confocal microscopy for the precise discrimination of tumorous brain tissue (such as glioblastoma, GBM) from normal tissue. However, it remains unclear if bright spot analysis can discriminate infiltrating tumor in the boundary zone and whether this method is suitable for GBM with no 5-ALA fluorescence or for other tumor types.

*Methods:* Brain tumor tissue resected from 5-ALA-treated patients was sectioned to evaluate bright spots under confocal microscopy with a 544.5 − 619.5 nm band-pass filter, which eliminated the fluorescence induced by 5-ALA. Border regions and adjacent normal tissues were observed for differences in bright spot distribution. Histopathology was also conducted by hematoxylin and eosin (H&E) staining of serial slices from the same samples to confirm the locations of tumorous, infiltrating, and normal regions. Bright spot areas were then calculated for the same regions evaluated by histopathology. This method was applied for GBM with and without 5-ALA-induced fluorescence as well as for lower-grade gliomas and other brain tumor types.

*Results:* The bright spot area was substantially smaller in the GBM body than in normal brain tissues. Bright spot area was also smaller in infiltrating tumors than in normal tissue at the margin. The same bright spot pattern was observed in tumorous tissues with no 5-ALA-induced fluorescence and in non-GBM tumors. The bright spot fluorescence is suggested to arise from lipofuscin based on emission spectra (mainly within 544.5 − 619.5 nm) and optimum excitation wavelength (about 405 nm).

*Conclusions:* Bright spot analysis is useful for discriminating infiltrating tumor from bordering normal tissue as an alternative or complement to photodynamic diagnosis with 5-ALA. This method is also potentially useful for tumors with no 5-ALA-derived red fluorescence and other nervous system tumors.

## 1. Introduction

Precise resection of glioblastoma (GBM) is critical for prolonging postoperative survival. On the other hand, excessive resection around the tumor may cause loss of neural function. It is thus crucial to differentiate between the tumor region to be removed and the normal region to be spared. Photodynamic diagnosis (PDD) using 5-aminolevulinic acid (5-ALA), first described by Stummer et al., is now widely used for the neurosurgical resection of brain tumors because it can greatly increase the tumor to normal tissue resection ratio [1–3]. Distinguishing tumor from healthy tissue is based on greater 5-ALA-derived protoporphyrin IX (PpIX) accumulation in glioma cells than non-cancer cells, resulting in much greater red fluorescence (peak at 635 nm) when excited at 405 nm [4].

There are many reports on the effectiveness of 5-ALA-derived fluorescence for identifying the main tumor prior to resection and for assessing the presence of residual tumor following resection [5–17]. However, it remains difficult to precisely distinguish the tumor margin and infiltrating regions from non-tumor tissue because the fluorescent boundary is usually vague. One potential solution proposed by Teng et al. is silencing ferrochelatase to enhance 5-ALA-derived fluorescence [18]. Another potential solution is the use of confocal microscopy due to its microscale resolution. Indeed, there have been several attempts to apply confocal microscopy for the resection of tumors [19–24]. Although confocal microscopy allows for the viewing of tumors at the microscale, it was not clear how infiltrating tumors appear in confocal

* Corresponding author.
*E-mail address:* yoneyama@se.kanazawa-u.ac.jp (T. Yoneyama).

https://doi.org/10.1016/j.pdpdt.2019.02.005
Received 1 November 2018; Received in revised form 11 January 2019; Accepted 4 February 2019
Available online 06 February 2019

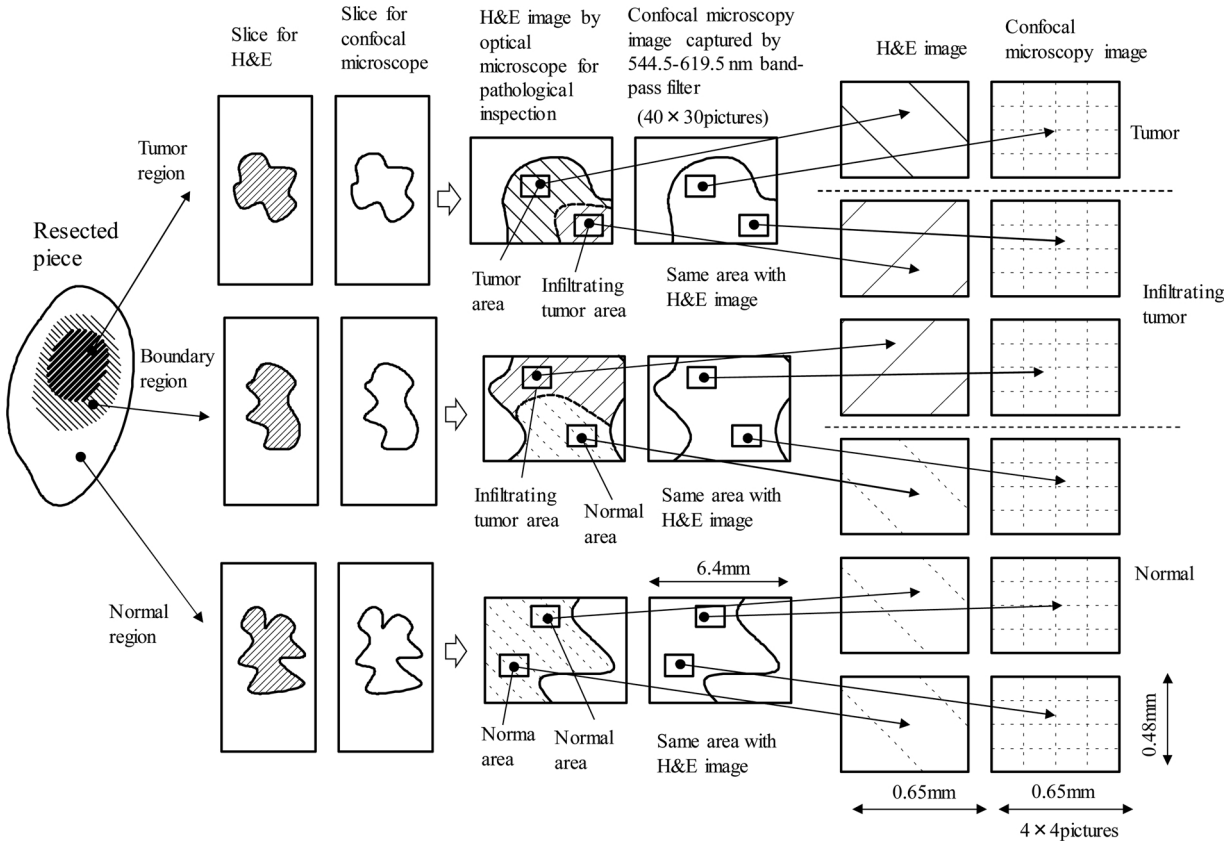


**Fig. 1.** Observation process from the resected specimen.

images and whether confocal microscopy is useful for distinguishing tumor tissue at the boundary with non-cancerous tissue.

We previously reported that fluorescence intensity analysis under confocal microscopy was useful for the discrimination of infiltrating tumor in the boundary area [25]. We also suggested that bright spot analysis was useful for tumor discrimination in a vague boundary area, but the source of bright spot fluorescence and the feasibility of bright spot analysis for different tumor types remain unclear. In this study, we examined resected brain specimens through a 544.5 − 619.5 nm band-pass filter to remove the 5-ALA-derived red fluorescence without interfering with the bright spot image. The bright spot area was then compared among tumor, infiltrating tumor, and normal tissue regions to investigate whether bright spot analysis can be used to distinguish tumors in marginal areas, tumors without 5-ALA-derived red fluorescence, and other brain tumors, including lower-grade gliomas.

## 2. Methods

### 2.1. Confocal microscopy-based bright spot analysis

For fluorescence analysis of specimens, we used a CSU22Z confocal laser-scanning microscope (Yokogawa Electric Corporation) and 405 nm D405C-50 laser at 50 mW (Showa Optronics). We compared images acquired using a 618.5–675.5 nm band-pass filter (usually used to detect red fluorescence such as from 5-ALA staining) with images acquired using a 544.5 − 619.5 nm band-pass filter (excluding red fluorescence) to examine the source of the bright spot. Fluorescence emission was captured by an electron-multiplying charge-coupled device camera (ANDOR/LucaS658 M) through an PlanApo 40×/NA 0.95 objective lens (OLYMPUS/UPLSAPO40 × 2). One confocal image contains 658 × 496 pixels and can capture a tissue area of 164.5 μm × 125 μm under this magnification. Therefore, the area of one pixel was about 0.25 μm × 0.25 μm in this study.

Precise positioning of the XY stage was required to construct multi-image maps. For this purpose, iQ software was used to move the stage and capture each image. For example, to acquire a fluorescence emission map of 6.4 mm × 3.7 mm, an array of 40 × 30 single images must be obtained. Using this system, a fluorescence map composed of detailed images could be obtained at the normal surgical microscope scale. Such a wide view was necessary to compare tissue fluorescence with hematoxylin and eosin (H&E) staining and to find the same tissue position for detailed comparisons at the microscale.

### 2.2. Specimens

Approximately 3 h before surgery, patients ingested a single dose of 20 mg kg body weight 5-ALA in 100 mL of juice. Resection was conducted following a standard microsurgical technique. Typically, the surgeon alternated between white and violet–blue light-emitting modes to visualize fluorescence during the resection. Tumor specimens were collected at various times during the procedure in both PpIX-positive (red fluorescent) and -negative regions. For patients with deep-seated GBMs underneath the cerebral cortex, tissue was resected from areas with invasion into normal brain. Samples containing a red fluorescent region, a surrounding non-fluorescent region, and a boundary were sent separately for pathological and confocal microscope examinations.

Six GBM samples with red fluorescence from six patients, three GBM samples with no red fluorescence from three patients, and several additional specimens from patient with other tumor types were obtained and analyzed. These additional specimens included two Grade III gliomas with red fluorescence, one Grade II glioma with no red fluorescence, one recurrent GBM, one nerve sarcoma with red fluorescence, and one normal tissue sample without 5-ALA staining.

### 2.3. Observation procedures

The observation process is shown in Fig. 1. Three 10-μm thick slices from the tumor region, boundary region, and normal brain region were cut from each tissue specimen in series. One slice was stained with H&E for pathological inspection using a normal optical microscope, while the second slice was examined by fluorescence confocal microscopy and the third was stored.

The H&E images were inspected by a skilled neurosurgeon and a pathologist to define tumor regions, infiltrating regions, and normal brain regions. Then, 0.65 mm × 0.48 mm areas were chosen to compare H&E images with fluorescence confocal microscopy images. Corresponding 0.65 mm × 0.48 mm areas were chosen for bright spot analysis. Each of these areas was captured by a 4 × 4 array of confocal microscopy images. Although the images were of different 10-μm thick cross-sections, nearly the same fluorescent pattern was observed in the slice before and following the slice used for H&E staining. Therefore, the distributions of tumor and normal tissue were well matched among 10-μm serial slices.

### 2.4. Bright spot analysis

Bright spot analysis included measurement of bright spot number, average size, size distribution, and total bright spot area. Bright spot analysis was performed on images filtered at 544.5 − 619.5 nm because only bright spots remained in this frequency band. Binarization was applied to confocal images according to a pixel intensity threshold determined independently for each resected specimen. Adjacent bright pixels were considered to be part of the same bright spot. The number of pixels included in one bright spot is referred to as the spot size. The number of bright spots larger than 40 pixels (2.5 $\mu m^2$) per image is defined as the bright spot number. Binarization for bright spot counting and size determination according to the assigned pixel intensity threshold was performed using an in-house computer algorithm. Bright spot area was calculated by multiplying average bright spot size and bright spot number. A raw image with bright spots and the same image after binarization are shown in Fig. 2. Rectangular areas of 0.65 mm × 0.48 mm (4 × 4 pictures) on the same area evaluated by histopathology were chosen in each region of the specimen for bright spot analysis.

## 3. Results

### 3.1. Comparison of confocal images band-pass filtered at 618.5–675.5 nm and 544.5–619.5 nm

Images of the same sample region obtained using a 618.5–675.5 nm band-pass filter and a 544.5–619.5 nm band-pass filter are shown in Fig. 3. This area contained tumor regions on both sides and an infiltrating tumor region in the center according to pathological inspection of the adjacent section by H&E staining. The fluorescence observed from the tumor region at 618.5–675.5 nm nearly disappeared when the image was filtered at 544.5–619.5 nm, while the same bright spots appeared in both images.

### 3.2. Bright spot analysis

(a) GBM with red fluorescence

Mean bright spot size, number, and total area are shown in the table of Fig. 4 for each GBM specimen with red fluorescence (Nos. 1 to 6). The appearance of the infiltrating region between normal and tumor tissue differed markedly among slices from different patients. Average bright spot areas in the tumor body, infiltrating tumor, and normal region were obtained from the acquired images. The ratios of the bright spot area in tumor and boundary areas to that in the normal tissue area were obtained for each sample. Acquiring the ratios effectively normalized for the high degree of variation in bright spot area among specimens. The ratio of the bright spot area in the tumor region to the normal region was quite small in all six specimens. The ratio of Bright spot areas in the infiltrating region were about 0.5 in samples 1 and 2, but were close to that of the normal region in samples 3 to 5 (i.e., a ratio of 1). The average bright spot ratio of tumor area to normal region and of infiltrating tumor to normal region for all GBM specimens with red fluorescence are shown as a column chart in Fig. 4(b).

As an example, H&E images and binarized bright spot confocal images are compared for specimen No. 1 (Fig. 4(c)). All three images are of the same boundary specimen. There are many more bright spots in the normal region and individual bright spot size is larger than in the tumor region.

(b) GBM with no red fluorescence

Bright spot size, number, and total area of each GBM sample with no red fluorescence (Nos. 7, 8, and 9) are shown in the table of Fig. 5. In these specimens, tumor and normal tissue were clearly distinguished by microscopic observation of H&E-stained sections. Average bright spot area was smaller in the tumor than the normal region of specimens 7 and 8, while bright spot area in specimen 9 was near zero. Comparing confocal images of specimen 8 to the corresponding H&E images confirmed greatly reduce bright spot number in the tumor compared to adjacent normal tissue (Fig. 5(c)).

(c) Other tumors

Bright spot size, number, and area in other samples (Nos. 10–15) are shown in the table of Fig. 6. Average bright spot area was smaller in the tumor than the normal region of specimens 10 and 11, both of which were Grade III glioblastomas. In the resected tumor region of specimen 12, a Grade II glioblastoma with no red fluorescence, bright spot area was also smaller than in the normal tissue. In the recurrent GBM specimen (No. 13), bright spot area was small in both the tumor and normal tissue, but was clearly larger in the normal tissue. In the nerve

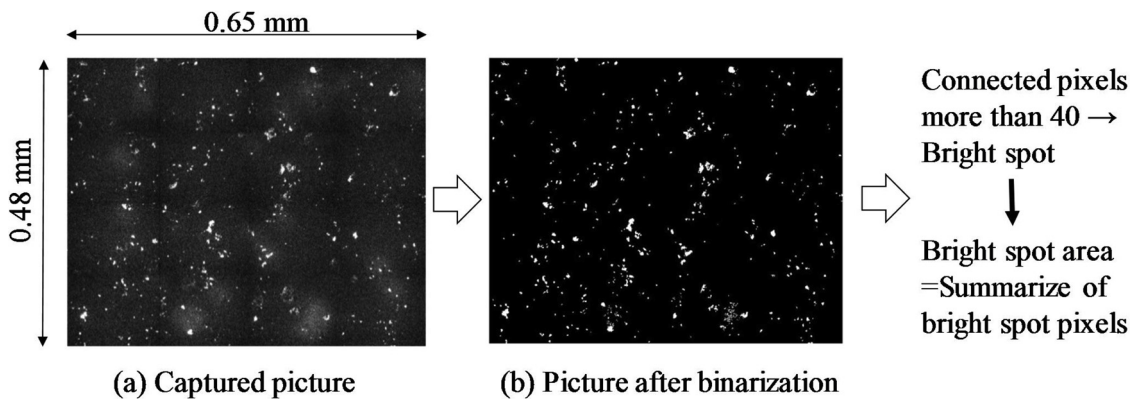


**Fig. 2.** Calculation method of bright spot area.

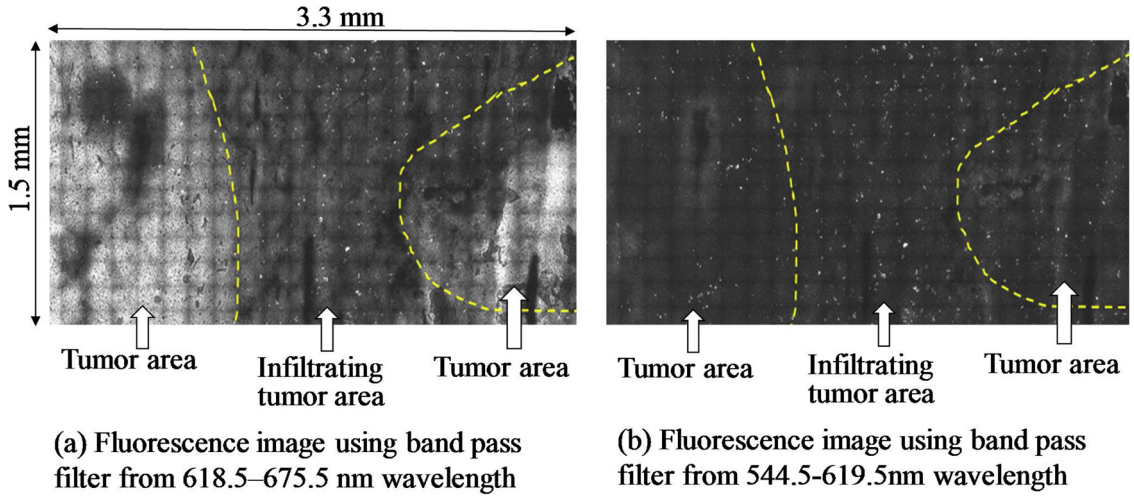


**Fig. 3.** Comparison between fluorescence image using band pass filter from 618.5 to 675.5 nm wavelength and that from 544.5 to 619.5 nm wavelength.

sarcoma sample (No. 14), the bright spot area in the tumor was also quite small compared to the normal region. In normal brain specimen 15 with no 5-ALA staining, the bright spot area was large. The small average ratio of bright spot area in tumor to normal tissue indicates that bright spot area was generally much higher in the normal tissue (Fig. 6(b)). As an example, the confocal image of the tumor area in specimen 12, a Grade II glioblastoma, was compared to that of the normal tissue area as defined by H&E (Fig. 6(c)). Many fewer and smaller bright spots were observed in the tumor region compared to the adjacent normal region.

## 4. Discussion

### 4.1. Source of the bright spot emission

The autofluorescence in the 544.5 − 619.5 nm range from 405 nm excitation may arise from lipofuscin, an aging-associated pigment produced in lysosomes and accumulated in granules within brain cells, cardiac muscle cells, and skin cells [26]. If lipofuscin is irradiated at 410 or 470 nm, it emits a fluorescence spectrum from 500 − 700 nm with a peak at 550 nm [27]. Previous reports indicated that the intracellular rate of lipofuscin formation increases in aging cells compared to younger or dividing cells [28]. In addition, the amount of lipofuscin was lower in intraepithelial neoplasia and malignant adenocarcinoma tissues than in benign hyperplasia tissue [29]. A previous *in vitro* study also found that normal glial cells contained larger amounts of lipofuscin than glioma cells [30]. In accord with these reports, our findings suggest that highly proliferating glioblastoma cells form little lipofuscin, resulting in fewer and smaller bright spots compared to normal brain tissue. While we cannot exclude other sources of bright spot emission, we are aware of no endogenous compounds with a similar fluorescence spectrum and tissue distribution. Further, these bright spots appeared independent of protoporphyrin IX fluorescence induced by 5-ALA staining.

### 4.2. Utility of bright spot analysis for distinguishing GBM with 5-ALA-derived fluorescence

Our main purpose was to investigate the utility of bright spot analysis for the precise discrimination of GBM at the boundary zone with normal tissue (the infiltrative zone) where fluorescence induced by 5-ALA is often poorly localized, at least with current microscopic techniques. The difference in bright spot area between tumor and normal region was very clear (Fig. 4). In GBM specimens containing the boundary region (specimens 1, 2, and 6), the bright spot area in infiltrating tumor was low. Therefore, bright spot analysis is helpful for the precise discrimination of brain tumor from healthy brain tissue at the microscale. Alternatively, in GBM specimens 3 and 5, the bright spot area of infiltrating tumor was close to that of normal tissues. However, the tumor with vague red fluorescence (specimen No. 3) was distinguished by the low bright spot area in the tumor sample. Thus, bright spot analysis may still be helpful for distinguishing tumors with poor 5-ALA staining at the microscale. In specimen No. 4, the bright spot area of the infiltrating region was much lower than in the normal region. Therefore, in the boundary samples, infiltrating tumor can also be distinguished by the difference in bright spot area.

Pathological grade determination is based on cell density and nuclear shape, and these features differed markedly among our samples. The relationship between bright spot area and cell density or nuclear shape in the tumor warrants further investigation to determine if bright spot analysis is also useful for tumor grading.

### 4.3. Utility of bright spot analysis for distinguishing GBM with no 5-ALA-derived fluorescence

We also assessed whether this method is useful for the discrimination of normal tissue from GBM with no 5-ALA-derived fluorescence. The boundary between tumor and normal tissue was clear in the histopathology samples. Further, the bright spot area was lower in the tumor than the normal tissue. Therefore, discrimination of tumor from normal tissue by bright spot analysis also appears possible for GBM with poor 5-ALA staining. However, this must be confirmed by observing many additional samples.

### 4.4. Utility of bright spot analysis for low-grade glioma and other tumors

Our third aim was to determine whether this method is useful for distinguishing low-grade glioma or other neural tumor types from surrounding healthy tissue. The bright spot area in Grade III glioma was clearly lower than in the surrounding normal tissue. Moreover, lower bright spot area was also observed in a Grade II glioma with no 5-ALA-derived red fluorescence. Therefore, discrimination of low-grade glioma at the microscale by bright spot analysis appears feasible. For the recurrent GBM (specimen No. 13), the bright spot area was small in both the tumor region and normal region but was clearly lower in the tumor region. Therefore, discrimination of the boundary zone was also possible. The bright spot area was also quite low in the nerve sarcoma specimen compared to surrounding normal tissue. Thus, discrimination by bright spot analysis may be possible for other nervous system tumors. The large bright spot area in normal tissue with no 5-ALA

(a) Bright spot size, number and area of each sample

| No. | Slice | Pathological inspection | Average size (pixels) | Bright spot number | Bright spot aera (average size × spot number) | Average spot area | Area ratio compared to each normal spot area | Red fluoresence observed by 618.5-675.5nm pass filter |
|---|---|---|---|---|---|---|---|---|
| 1 | Boundary | Tumor | 165 | 185 | 30525 | 30525 | 0.33 | clear |
| | | Infiltrating tumor | 268 | 219 | 58714 | 45280 | 0.50 | vague |
| | | Infiltrating tumor | 159 | 244 | 38820 | | | |
| | | Infiltrating tumor | 214 | 179 | 38306 | | | |
| | | Normal | 343 | 247 | 84820 | 91339 | 1 | no |
| | Normal | Normal | 209 | 468 | 97859 | | | |
| 2 | Tumor | Tumor | 205 | 12 | 2456 | 2456 | 0.04 | vague |
| | Boundary | Infiltrating tumor | 162 | 193 | 31189 | 31189 | 0.53 | no |
| | | Normal | 138 | 404 | 55914 | 59402 | 1 | no |
| | Normal | Normal | 121 | 330 | 39930 | | | |
| | | Normal | 130 | 636 | 82362 | | | |
| 3 | Tumor | Tumor | 309 | 75 | 23205 | 26430 | 0.35 | vague |
| | | Tumor | 195 | 152 | 29655 | | | |
| | Boundary | Infiltrating tumor | 122 | 769 | 93434 | 72191 | 0.96 | no |
| | | Infiltrating tumor | 115 | 539 | 61823 | | | |
| | | Infiltrating tumor | 112 | 546 | 61316 | | | |
| | Normal | Normal | 314 | 240 | 75408 | 75408 | 1 | no |
| 4 | Tumor | Tumor | 152 | 10 | 1519 | 1519 | 0.02 | strong |
| | Boundary | Infiltrating tumor | 288 | 264 | 76111 | 80986 | 0.96 | no |
| | | Infiltrating tumor | 180 | 477 | 85860 | | | |
| | | Normal | 173 | 768 | 133094 | 84240 | 1 | no |
| | | Normal | 172 | 604 | 103707 | | | |
| | Normal | Normal | 316 | 193 | 60892 | | | |
| | | Normal | 244 | 161 | 39268 | | | |
| 5 | Tumor | Tumor | 96 | 5 | 480 | 480 | 0.01 | strong |
| | Boundary | Infiltrating tumor | 214 | 368 | 78789 | 68386 | 0.83 | clear |
| | | Infiltrating tumor | 109 | 817 | 88971 | | | no |
| | | Infiltrating tumor | 101 | 371 | 37397 | | | no |
| | Normal | Normal | 223 | 365 | 81286 | 82544 | 1 | no |
| | | Normal | 265 | 316 | 83803 | | | |
| 6 | Boundary | Tumor | 108 | 193 | 20767 | 20767 | 0.13 | strong |
| | | Normal | 385 | 468 | 180040 | 157720 | 1 | no |
| | | Normal | 340 | 398 | 135400 | | | |

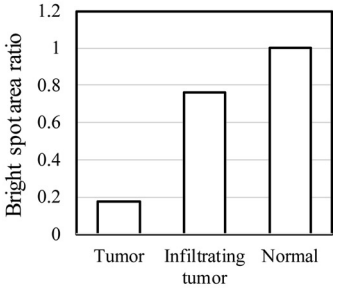


(b) Ratio of average bright spot area to normal

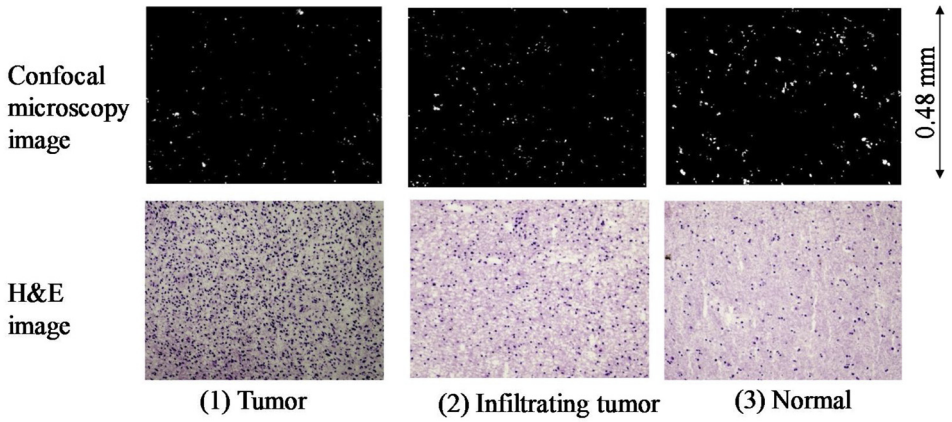


(c) Example of H&E image and confocal microscopy image (Specimen No.1)

**Fig. 4.** Ratio of the bright spot area in tumor to that in normal in GBM with red fluorescence.

administration supports the idea that bright spots are not induced by 5-ALA.

### 4.5. Comparison of bright spot areas among all observed samples

Our results suggest that bright spot analysis may be a useful alternative to 5-ALA fluorescence. First, the distinct emission spectra

(a) Bright spot size, number and area of each sample

| No. | Slice | Pathological inspection | Average size (pixels) | Bright spot number | Bright spot aera (average size × spot number) | Average spot area | Area ratio compared to each normal spot area |
|---|---|---|---|---|---|---|---|
| 7 | Boundary | Tumor | 123.5 | 248 | 30628 | 24873 | 0.76 |
| | | Tumor | 163.4 | 117 | 19118 | | |
| | | Normal | 241.3 | 227 | 54775 | 32593 | 1 |
| | | Normal | 212.1 | 130 | 27573 | | |
| | Normal | Normal | 277.4 | 120 | 33288 | | |
| | | Normal | 241.6 | 61 | 14738 | | |
| 8 | Boundary | Tumor | 106.6 | 304 | 32406 | 31409 | 0.62 |
| | | Tumor | 120.2 | 253 | 30411 | | |
| | | Normal | 132.9 | 426 | 56615 | 51043 | 1 |
| | | Normal | 217.6 | 268 | 58317 | | |
| | Normal | Normal | 206.3 | 243 | 50131 | | |
| | | Normal | 174.6 | 224 | 39110 | | |
| 9 | Tumor | Tumor | 88.5 | 2 | 177 | 177 | 0.00 |
| | Boundary | Normal | 109.2 | 808 | 88234 | 68051 | 1 |
| | | Normal | 103.8 | 607 | 63007 | | |
| | Normal | Normal | 109.4 | 389 | 42557 | | |
| | | Normal | 175.8 | 446 | 78407 | | |

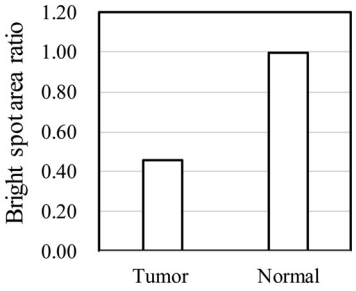


(b) Ratio of average bright spot area to normal

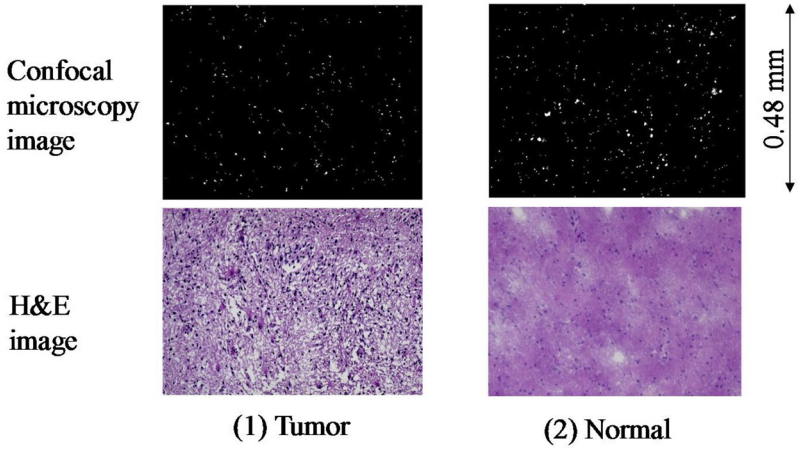


(c) Example of H&E image and confocal microscopy image (Specimen No.8)

**Fig. 5.** Ratio of the bright spot area in tumor to that in normal in GBM with no red fluorescence.

indicates that protoporphyrin IX fluorescence induced by 5-ALA is not the source of these bright spots. Also, reduced bright spot area was observed in most tumors, even those with poor 5-ALA fluorescence. To test the general utility of bright spot analysis, we compared the average ratios of tumor body to normal tissue bright spot area and infiltrating tumor to normal tissue bright spot area for all 41 specimens (Fig. 7). The bright spot area ratios of 21 main tumor samples and 12 infiltrating tumors are plotted as columns in Fig. 7. Unpaired *t*-test indicated significant differences between normal and infiltrating tumor ($p < 0.05$), between main tumor and normal tissue ($p < 0.01$), and between main tumor and infiltrating tumor ($p < 0.01$), indicating the feasibility of bright spot analysis for the discrimination of many tumor types. Of course, more detail investigations will be necessary to assess utility for other tumors.

### 4.6. Microlocation of bright spots

In this paper, we compared the bright spot images from confocal microscopy with H&E images at high magnification. However, as the nuclear diameter is smaller than the slice thickness (10 μm), the same nuclei would not appear in H&E samples and confocal microscopy images. Therefore, we could not directly compare bright spot location with nuclear location. However, we have once compared the location of bright spots to nuclear positions using the same slices, first processed for confocal microscopy and then for H&E staining. The study indicated the location of the bright spots were near the location of nucleus but the bright spots were not in the nucleus and were not in blood cells. Further investigation will be necessary to define the source of these bright spots and their behavior during tumor progression.

(a) Bright spot size, number and area of each sample

| No. | Slice | Pathological inspection | Average size (pixels) | Bright spot number | Bright spot aera (average size × spot number) | Average spot area | Area ratio compared to each normal spot area | Tumor type |
|---|---|---|---|---|---|---|---|---|
| 10 | Tumor | Tumor | 247 | 13 | 3208 | 2269 | 0.03 | Grade Ⅲ glioma with red fluorescence |
| | | Tumor | 89 | 15 | 1331 | | | |
| | Normal | Normal | 242 | 180 | 43596 | 77663 | 1 | |
| | | Normal | 295 | 379 | 111729 | | | |
| 11 | Tumor | Tumor | 126 | 126 | 15851 | 13085 | 0.21 | Grade Ⅲ glioma with red fluorescence |
| | | Tumor | 113 | 91 | 10319 | | | |
| | Boundary | Infiltrating tumor | 124 | 119 | 14697 | 16125 | 0.26 | |
| | | Infiltrating tumor | 127 | 138 | 17554 | | | |
| | Normal | Normal | 174 | 338 | 58947 | 61374 | 1 | |
| | | Normal | 188 | 339 | 63800 | | | |
| 12 | Tumor | Tumor | 197 | 125 | 24663 | 24663 | 0.31 | Grade Ⅱ glioma with no red fluorescence |
| | | Normal | 456 | 174 | 79274 | 79274 | 1 | |
| 13 | Boundary | Tumor | 113 | 322 | 36483 | 39141 | 0.40 | Recurred tumor with red fluorescence |
| | | Tumor | 134 | 311 | 41798 | | | |
| | | Normal | 209 | 306 | 63832 | 97969 | 1 | |
| | | Normal | 158 | 201 | 31778 | | | |
| | Normal | Normal | 165 | 692 | 114180 | | | |
| | | Normal | 201 | 905 | 182086 | | | |
| 14 | Tumor | Tumor | 237 | 14 | 3324 | 2871 | 0.06 | Nerve sarcoma with red fluorescence |
| | | Tumor | 151 | 16 | 2418 | | | |
| | Boundary | Normal | 274 | 144 | 39427 | 48385 | 1 | |
| | | Normal | 234 | 229 | 53586 | | | |
| | Normal | Normal | 190 | 231 | 43890 | | | |
| | | Normal | 229 | 247 | 56637 | | | |
| 15 | Normal | Normal | 337 | 390 | 131547 | 135707 | | Normal brain with no 5-ALA |
| | | Normal | 303 | 461 | 139867 | | | |

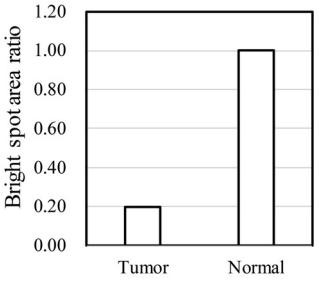


(b) Ratio of average bright spot area to normal

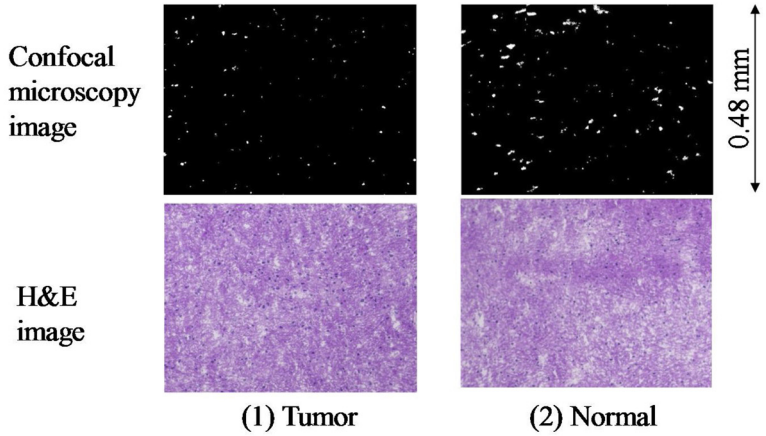


(c) Example of H&E image and confocal microscopy image (Specimen No.12)

**Fig. 6.** Ratio of the bright spot area in tumor to that in normal in other specimens.

### *4.7. Role of bright spot analysis in 5-ALA fluorescence diagnosis*

As we investigated in the previous paper [25], fluorescence intensity analysis is very useful for localization of brain tumors. Infiltrating tumors emit more intense 5-ALA-derived red fluorescence than normal brain tissue. However, many infiltrating tumors and tumors in the boundary are low emitting. Bright spot analysis may thus be a helpful alternative approach to distinguish tumor from normal tissue at the boundary area or to locate infiltrating tumor areas. In our previous study, we did not notice that bright spot intensity is independent of 5-ALA-induced fluorescence. Therefore, this previous bright spot analysis was performed on images captured with a 618.5–675.5 nm band-pass filter and thus including both 5-ALA-induced fluorescence signals and bright spots. In the example bright spot analysis of that study, we compared tissues using average bright spot size and bright spot number, but we have since noticed that the most reliable tumor marker is reduced bright spot area compared to the adjacent normal tissue. Therefore, we compared tissues using bright spot area in this paper. By adding bright spot analysis as shown in this paper, even tumors without clear 5-ALA-induced fluorescence can be reliability distinguished.

This technology will help neurosurgeons more accurately define the border between normal brain and infiltrating tumor tissue before resection, thereby enhancing functional preservation of normal tissue and reducing recurrence rates.

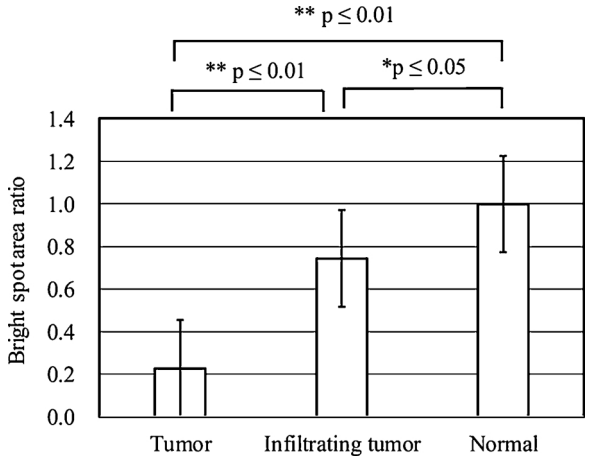


**Fig. 7.** Comparison of bright spot area in all the specimen.

## 5. Conclusions

Brain tissue bright spots at 544.5 − 619.5 nm from 405 nm laser excitation were examined for their utility to distinguish glioblastoma multiforme (GBM) with red fluorescence from 5-ALA staining, GBM with no red fluorescence from 5-ALA staining, and other tumor specimens from the surrounding boundary and normal tissue regions. The bright spot area was generally lower in the tumor than the normal region, suggesting possible utility for discrimination of tumor and infiltrating areas from normal brain tissue. Moreover, this method appeared useful from GBM, lower-grade gliomas, and other nervous system tumors. We speculate that bright spots are due to lipofuscin fluorescence. The mechanism for bright spot fluorescence reduction in tumors and the utility of this phenomenon for the precise discrimination of other brain tumors warrants further investigation.

## Funding

This research was supported by JSPS KAKENHI Grant Number 26242054.

## Conflict of interest

The authors declare that they have no conflict of interest.

## Ethical approval

This study was approved by the Ethics Committee of Kanazawa University (No. 209-7).

## Informed consent

Informed consent was obtained from all individual participants included in the study.

## Acknowledgments

The authors thank Naomichi Ishikawa, a former master course student at Kanazawa University, for cooperation in the progress of this research. The authors also thank Hemuragul Sabit for help with pathological inspection of the resected specimens.

## References

[1] W. Stummer, S. Stocker, S. Wagner, H. Stepp, C. Fritsch, C. Goetz, A.E. Goetz, R. Kiefmann, H.J. Reulen, Intraoperative detection of malignant gliomas by 5-aminolevulinic acid-induced porphyrin fluorescence, Neurosurgery 42 (1998) 518–526.
[2] W. Stummer, A. Novotny, H. Stepp, C. Goetz, K. Bise, H.J. Reulen, Fluorescence-guided resection of glioblastoma multiforme by using 5-aminolevulinic acid—induced porphyrins: a prospective study in 52 consecutive patients, J. Neurosurgery 93 (2000) 1003–1013.
[3] W. Stummer, U. Pichlmeier, T. Meinel, O.D. Wiestler, F. Zanella, H.J. Reulen, Fluorescence-guided surgery with 5-aminolevulinic acid for resection of malignant glioma: randomized controlled multicenter phase III trial, Lancet Oncol. 7 (2006) 392–401.
[4] W. Stummer, S. Stocker, A. Novotny, A. Heimann, O. Sauer, O. Kempski, N. Pressnilla, J. Wietzorrek, H.J. Reulen, In vitro and in vivo porphyrin accumulation by C6 glioma cells after exposure to 5-aminolevulinic acid, J. Photochem. Photobiol. B 45 (1998) 160–169.
[5] S. Kaneko, I. Okura, T. Tanaka, Photodynamic Applications (PDD, PDT) Using Aminolevulinic Acid in Neurosurgery, Aminolevulinic Acid, SBI ALApromo, 2015, pp. 119–140.
[6] S. Kaneko, S. Kaneko, Fluorescence-guided resection of malignant glioma with 5-ALA, Int. J. Biomed. Imaging 2016 (2016) 1–11.
[7] P.P. Panciani, M. Fontanella, B. Schatlo, D. Garbossa, A. Agnoletti, A. Ducat, M. Lanotte, Fluorescence and image guided resection in high grade glioma, Clin. Neurol. Neurosurg. 114 (1) (2012) 37–41.
[8] R. Diez Valle, S. Tejada Solis, M.A. Idoate Gastearena, R.Garcia de Eulate, P. Dominguez Echavarri, J. Aristu Mendiroz, Surgery guided by 5-aminolevulinic fluorescence in glioblastoma: volumetric analysis of extent of resection in single-center experience, J. Neurooncol. 102 (2011) 105–113.
[9] D.W. Roberts, P.A. Valdes, B.T. Harris, K.M. Fontaine, A. Hartov, X. Fan, S. Ji, S.S. Lollis, B.W. Pogue, F. Leblond, T.D. Tosteson, B.C. Wilson, K. Paulsen, Coregistered fluorescence-enhanced tumor resection of malignant glioma: relationship between δ-aminolevulinic acid-induced protoporphyrin IX fluorescence, magnetic resonance imaging enhancement, and neuropathological parameters. Clinical article, J. Neurosurg. 114 (2011) 595–603.
[10] M. Hefti, G. von Campe, M. Moschopulos, A. Siegner, H. Looser, H. Landolt, 5-aminolevulinic acid induced protoporphyrin IX fluorescence in high-grade glioma surgery: a one-year experience at a single institution, Swiss Med. Wky 138 (2008) 180–185.
[11] M. Hefti, H.M. Mehdorn, I. Albert, L. Dörner, Fluorescence-guided surgery for malignant glioma: a review on aminolevulinic acid induced protoporphyrin IX photodynamic diagnostic in brain tumors, Curr. Med. Imaging Rev. 6 (2010) 1–5.
[12] S. Eljamel, Photodynamic applications in brain tumors: a comprehensive review of the literature, Photodiagn. Photodyn. Ther. 7 (2010) 76–85.
[13] W. Stummer, J.C. Tonn, C. Goetz, W. Ullrich, H. Stepp, A. Bink, T. Pietsch, U. Pichlmeier, 5-aminolevulinic acid-derived tumor fluorescence: the diagnostic accuracy of visible fluorescence qualities as corroborated by spectrometry and histology and postoperative imaging, Neurosurgery 74 (2014) 310–319.
[14] S. Utsuki, H. Oka, S. Sato, S. Suzuki, S. Shimizu, S. Tanaka, K. Fujii, Possibility of using laser spectroscopy for the intraoperative detection of nonfluorescing brain tumors and the boundaries of brain tumor infiltrates, Technical note, J. Neurosurg. 104 (2006) 618–620.
[15] K. Roessler, A. Becherer, M. Donat, M. Cejna, I. Zachenhofer, Intraoperative tissue fluorescence using 5-aminolevulinic acid (5-ALA) is more sensitive than contrast MRI or amino acid positron emission tomography ((18)F-FET PET) in glioblastoma surgery, Neurol. Res. 34 (2012) 314–317.
[16] G. Widhalm, B. Kiesel, A. Woehrer, T. Traub-Weidinger, M. Preusser, C. Marosi, D. Prayer, J.A. Hainfellner, E. Knosp, S. Wolfsberger, 5-Aminolevulinic acid induced fluorescence is a powerful intraoperative marker for precise histopathological grading of gliomas with non-significant contrast-enhancement, PLoS One 8 (2013) e76988.
[17] G. Widhalm, S. Wolfsberger, G. Minchev, A. Woehrer, M. Krssak, T. Czech, D. Prayer, S. Asenbaum, J.A. Hainfellner, E. Knosp, 5-Aminolevulinic acid is a promising marker for detection of anaplastic foci in diffusely infiltrating gliomas with nonsignificant contrast enhancement, Cancer 116 (2010) 1545–1552.
[18] L. Teng, M. Nakada, S.-G. Zhao, Y. Endo, N. Furuyama, E. Nambu, I.V. Pyko, Y. Hayashi, J.I. Hamada, Silencing of ferrochelatase enhances 5-aminolevulinic acid-based fluorescence and photodynamic therapy efficacy, Br. J. Cancer 104 (2011) 798–807 19.
[19] N. Sanai, L.A. Snyder, N.J. Honea, S.W. Coons, J.M. Eschbacher, K.A. Smith, R.F. Spetzler, Intraoperative confocal microscopy in the visualization of 5-aminolevulinic acid fluorescence in low-grade gliomas, J. Neurosurg. 115 (2011) 740–748.
[20] J. Eschbacher, N.L. Martirosyan, P. Nakaji, N. Sanai, M.C. Preul, K.A. Smith, S.W. Coons, R.F. Spetzler, In vivo intrraperative confocal microscopy for real-time histopathological imaging of brain tumors, J. Neurosurg. 116 (2012) 854–860.
[21] N.L. Martirosyan, J. Georges, J.M. Eschbacher, D.D. Cavalcanti, A.M. Elhadi, M.G. Abdelwahab, A.C. Scheck, P. Nakaji, R.F. Spetzler, M.C. Peul, Potential application of a handheld confocal endomicroscope imaging system using a variety of fluorophores in experimental gliomas and normal brain, Neurosurg. Focus 36 (2014) 1–14.
[22] M.A. Mooney, A.H. Zehri, J.F. Georges, P. Nakaji, Laser scanning confocal microscopy in the neurosurgical operating room: a review and discussion of future applications, Neurosurg. Focus 36 (2) (2014).
[23] J. Liu, D. Meza, N. Sanai, Trends in fluorescence image-guided surgery for gliomas, Neurosurgery 75 (2014) 61–71.
[24] C.G. Hadjipanayis, G. Widhalm, W. Stummer, What is the surgical benefit of utilizing 5-aminolevulinic acid for fluorescence-guided surgery of malignant gliomas? Neurosurgery 77 (2015) 663–673.
[25] T. Yoneyama, H. Kagawa, T. Watanabe, Y. Hayashi, M. Nakada, Fluorescence

intensity and bright spot analysis using a confocal microscope for photodynamic diagnosis of brain tumors, Photodiagnosis Photodyn. Ther. 17 (2017) 13–21.
[26] H. Schönenbrücher, R. Adhikary, P. Mukherjee, T.A. Casey, M.A. Rasmussen, F.D. Maistrovich, A.N. Hamir, M.E. Kehrli Jr., J.A. Richt, J.W. Petrich, Fluorescence-Based Method, Exploiting Lipofuscin, for Real-Time Detection of Central Nervous System Tissues on Bovine Carcasses, Agric. Food Chem. 56 (2008) 6220–6226.
[27] A.M. García, A. Kun, O. Calero, M. Medina, M. Calero, An overview of the role of Lipofuscin in age-related neurodegeneration, Front. Neurosci. 12 (464) (2018) 1–13.
[28] T. Jung, N. Bader, T. Grune, Lipofuscin: formation, distribution, and metabolic consequences, Ann. N. Y. Acad. Sci. 1119 (2007) 97–111.
[29] J.B. Brennick, J.X. O'Connell, G.R. Dickersin, B.Z. Pilch, R.H. Young, Lipofuscin pigmentation (so-called "melanosis") of the prostate, Am. J. Surg. Pathol. 18 (1994) 446–454.
[30] H.H. Thaw, Optimal conditions for the measurement of lipid peroxidation products (lipofuscin) in individual cultivated human glial and glioma cells, Mech. Ageing Dev. 38 (1987) 79–87.